ACS OMEGA

Open Access

http://pubs.acs.org/journal/acsodf

Article

Pharmaceutical Properties of the Phloretin−4,4′-Bipyridine Cocrystal: Structure Analysis, Drug Release Profile, and Antioxidant Activity Research

Zhongyu Lu, Gengzhen Yao, Huanglie Xie, Dawei Wang, Yanfen Chen,* and Wei Zhu*

Cite This: *ACS Omega* 2024, 9, 31477−31487

Read Online

ACCESS | Metrics & More | Article Recommendations | Supporting Information

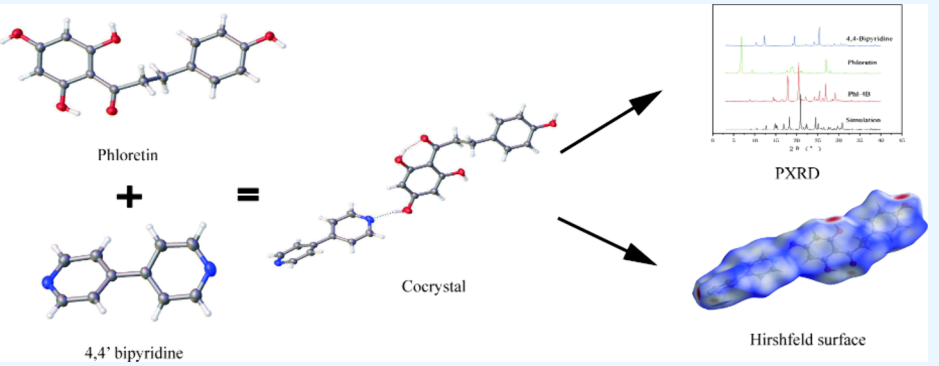

ABSTRACT: To improve the water solubility of phloretin, we synthesized the Phl−4B cocrystal using the solvent evaporation method. Various analytical techniques including powder X-ray diffraction (PXRD), thermogravimetric analysis (TGA), differential scanning calorimetry (DSC), Fourier transform infrared (FTIR), ^{1}HNMR, and single-crystal X-ray diffraction (SCXRD) were employed to evaluate the crystal thermodynamics and structure. The results of PXRD and SCXRD showed that it was a new cocrystal crystallized in the *P*-1 space group of the triclinic system. Thermal analysis confirmed the purity of the Phl−4B cocrystal. The equilibrium solubility of the Phl−4B cocrystal in pH 1.2 was improved. In vitro simulated digestion experiments indicated that the release of the Phl−4B cocrystal followed Fick diffusion. The stability activity of phloretin after pharmaceutical cocrystallization was improved. The antioxidant of the Phl−4B cocrystal was better than that of pure Phl.

INTRODUCTION

Many of the drugs with good therapeutic effects are BCS II and BCS IV types, which limit their therapeutic effectiveness and lot of research on improving the water solubility of drugs.[1−3] When the crystal structure of the drug is changed, its solubility, dissolution, stability, and thermodynamic parameters will be changed.[4] Pharmaceutical cocrystallization is a process in which the pharmaceutical ingredient (API) and cocrystal former (CCF) form a crystal in the same lattice through noncovalent formation to change its crystal structure.[5−7] Therefore, pharmaceutical cocrystallization is one of the methods that can be used to improve the water solubility of drugs.[8,9]

Phloretin is a flavonoid (Figure 1a) mainly found in apples or pears, which has anticancer,[10,11] antiobesity,[12] anti-inflammation,[11,13] antioxidant,[14] and antidiabetes[15] effects. The reason for its poor water solubility is the strong hydrogen bonding between the molecules of phloretin, which also leads to its low bioavailability. Therefore, we consider using a pharmaceutical cocrystal to improve the water solubility of phloretin.

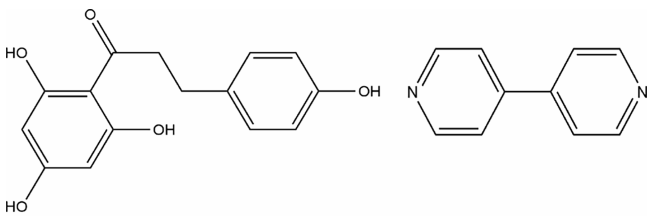

(a) (b)

Figure 1. Chemical structure of phloretin (a) and 4,4′-bipyridine (b).

Our research group is committed to using this strategy to improve the water solubility of natural compounds. In the preliminary experiment,[16] our research group found that

Received: February 4, 2024
Revised: May 26, 2024
Accepted: June 17, 2024
Published: July 8, 2024

phloretin could form a cocrystal with isoniazid (Figure 2). After the cocrystal formation of phloretin and isoniazid, the

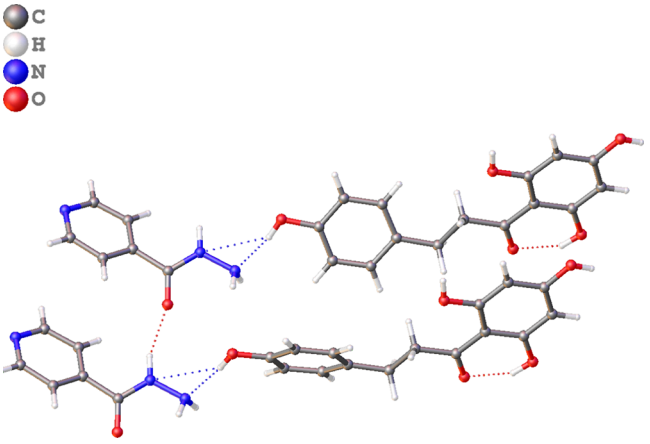

Figure 2. Crystal structure of the Phl−Inz cocrystal.

water solubility of phloretin improved. However, isoniazid was inherently toxic; we continued screening more compounds as a more suitable CCF. Surprisingly, we found that phloretin could form a cocrystal with 4,4′-bipyridine (Figure 1b); thus, the new cocrystal was the research objective. In this work, we studied the thermodynamic parameters, structural characterization, and intermolecular forces of the Phl−4B cocrystal. In addition, the water solubility, release rule, stability, and antioxidant activity of the cocrystal were studied subsequently. The Phl−4B cocrystal demonstrates that Phl can form a cocrystal with substances sharing a similar structure to 4B, thereby offering valuable insights into subsequent cocrystal design.

RESULTS AND DISCUSSION

PXRD Analysis. PXRD could be performed for the formation of a new crystal phase to describe the characteristic of a cocrystal.[17] The PXRD patterns of Phl, 4B, and Phl−4B cocrystals are shown in Figure 3. The pattern of 4B had characteristic diffraction peaks at 10.4°, 12.3°, 19.4°, 24.2° and 25.4°. The diffraction peaks of the cocrystal were 17.9°, 20.5°, 22.1°, 24.2°, 25.4°, 26.2°, 26.9° and 29.1°, which were basically with its simulated PXRD form single-crystal diffraction pattern. Moreover, the pattern of Phl showed peaks of 9°, 9.4°, 13.8°, 16.4°, 17.7°, 27.0° and 27.9°. It could be seen that 17.9° and 20.5° of the Phl−4B cocrystal were the new characteristic diffraction peaks different from those of Phl and 4B, which showed that it was a new crystalline phase. In addition, the pattern of the cocrystal was similar to the simulated pattern calculated from SCXRD data, which confirmed the new cocrystal.

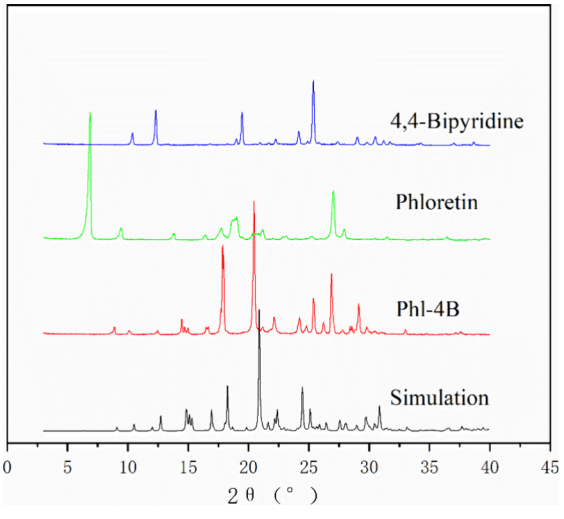

Figure 3. PXRD patterns of each sample.

Thermal Analysis. Differential scanning calorimetry (DSC) and thermogravimetric analysis (TGA) could be used to examine the thermal behavior of a cocrystal.[18,19] The purity of the component could be judged by the melting point measured by DSC, and TGA could be used to analyze whether the substance was a solvent compound by the mass change of the tested substance over a temperature range. Based on previous experiments, Phl had a unique endothermic peak at 266.9 °C by DSC (Figure 4). It could be seen in the DSC curve that 4B had a sharp endothermic peak appearing at approximately 111.5 °C. After the formation of cocrystal Phl

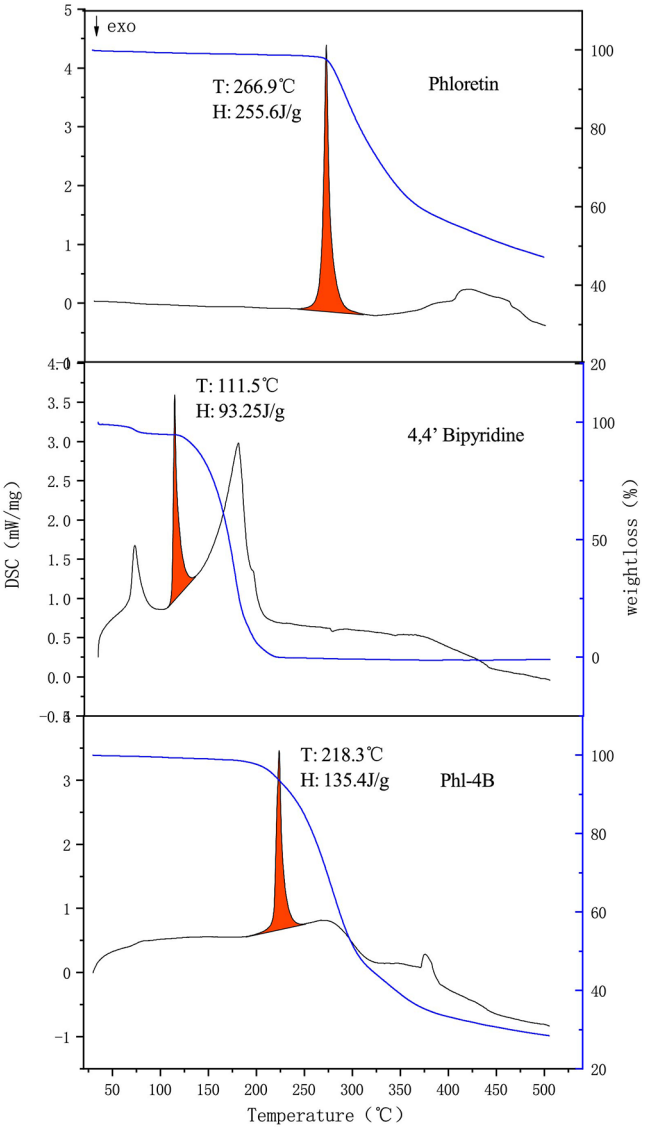

Figure 4. DSC and TGA curves.

https://doi.org/10.1021/acsomega.4c01136
ACS Omega 2024, 9, 31477−31487

and 4B, DSC results of the Phl−4B cocrystal showed that it had a new endothermic peak at 218.3 °C, which was different from those of Phl and 4B. Moreover, the enthalpy values of Phl, 4B, and Phl−4B cocrystal were 255.6 J/g, 93.25 J/g and 135.4 J/g, respectively. This meant that Phl−4B was a new crystal. According to the TGA curve, there was no obvious weight-loss platform in the Phl−4B curve, indicating that no solvent molecules were precipitated so it was not solvated.

FTIR Analysis. When Phl and 4B formed a cocrystal through a noncovalent bond such as hydrogen bond, the vibration energy of related functional groups changed under the influence of the noncovalent bond, resulting in a certain degree of change in the Fourier transform infrared spectroscopy.[20] In the infrared spectrum (Figure 5), Phl appeared with

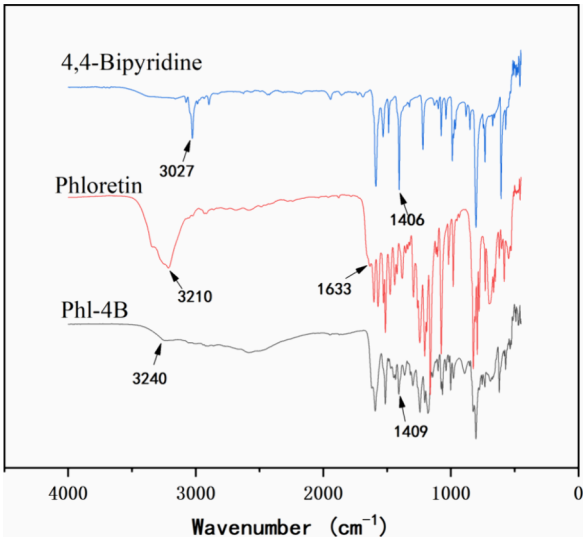

Figure 5. FTIR of Phl, 4B, and Phl-4B.

characteristic peaks at 3210 and 1633 cm^{-1}, corresponding to the O−H and C═O stretching vibrations of hydroxyl and carbonyl groups. Moreover, 4B showed characteristic peaks at 3027 and 1406 cm^{-1} corresponding to C−H and C═N on the pyridine ring. In the cocrystal, stretching vibrations of the ions of O−H shifted to 3240 cm^{-1} from 3210 cm^{-1} and the stretching vibration peak at 1409 cm^{-1} was basically the same as that of 4B, which were caused by the hydrogen bond between O−H of Phl and the ions of 4B.

^{1}HNMR Analysis. The ratio of each component could be determined by the integral of the characteristic peak of each component in ^{1}HNMR.[21−23] As shown in Figure 6, the chemical shifts of characteristic peaks of Phl in the cocrystal were as follows (red point): δ12.24 (s, 2H), 10.35 (s, 1H), 9.14 (s, 1H), 7.02 (d, J = 8.4 Hz, 2H), 6.67 (d, J = 8.4 Hz, 2H), 5.82 (s, 2H), 3.22 (t, J = 7.8 Hz, 2H), 2.77 (t, J = 7.8 Hz, 2H). For 4B, the ^{1}HNMR is as follows (blue point): δ10.10 (s, 1H), 8.71 (d, J = 6.1 Hz, 2H), 7.73 (d, J = 6.1 Hz, 2H), 4.63 (s, 2H). According to the integration results of Phl and 4B characteristic peaks in the ^{1}HNMR, the ratio of Phl and 4B in the cocrystal was 1:1, which was consistent with the calculated material ratio. Solid-state NMR emerges as one of the most suitable methods for characterizing cocrystals.[24,25] Due to the limitation of our experimental conditions, solid-state NMR was not utilized for cocrystal characterization. Subsequently, in follow-up experiments, solid-state NMR will be employed to supplement the pertinent data by characterizing the crystals.

Crystal Structure Determination. SCXRD could be used to obtain information about the exact three-dimensional structure and molecular arrangement of compounds.[26,27] Cocrystal Phl−4B was crystallized in the *P-1* space group (Table 1) of the triclinic system, which contained one molecule of Phl and one molecule of 4B in the asymmetric unit (Figure 7a). The unit cell consisted of two asymmetric units (Figure 7b), and more data of hydrogen-bonding distances and angles for the cocrystal are shown in Table 2. As shown in Figure 7c, each molecule of Phl was associated with the adjacent 4B through the ligands of the enantiomer through O1−H1··· N2 and O4−H4··· N1 formed hydrogen bonds extending in one dimer. These dimers contacted with each other by O5−H5A··· O1 hydrogen bonds of O1 forming long two-dimensional planar structures (Figure 7d). Interaction of H···π was found in the cocrystal, which was from C25−H25 to Cg1 at (−1+x, y, z), and the perpendicular distance of H to the ring plan was 2.854 (Figure 8). Meanwhile, there was π···π stacking in the structure, which was from Cg1 at (x, y, z) to Cg2 at (1+x, y, z). The interplanar distances between the relevant centroids demonstrate a slippage angle of 10.17 for Cg1···Cg2, which showed the J-type π···π stacking structure (Figure 9). In addition, the centroid−centroid distance was 3.814 and the shift distance was 1.417. Finally, by the intermolecular force of π−π stacking, each two-dimensional planar structure was alternately stacked into a three-dimensional structure.

Hirshfeld Surface Analysis. The Hirshfeld surface of the cocrystal could be analyzed to observe the interaction between the components in the cocrystal more clearly.[28,29] According to the space occupied by molecules in the crystal, the surface of Hirshfeld divides different molecular fragments according to the electron density of the crystal and then analyzes the intermolecular interaction force and visualizes the types and regions of intermolecular contact in the crystal. The Hirshfeld surface of the cocrystal and the corresponding two-dimensional fingerprint were generated by CrystalExplorer 21.5. d_i and d_e respectively represent the closest distance between the atoms inside the surface and the closest distance between the atoms outside the surface, while d_{norm} measures the contact distance between molecules in the corresponding region.[30] The red and blue colors of the Hirshfeld surface diagram represent the high and low intensities of the intermolecular forces, respectively, which visualize the strength of the d_{norm} points and then provide important information about the intermolecular interactions.

The Hirshfeld surfaces of the cocrystal are shown in Figure 10a. The d_{norm} map of the cocrystal with a red spot explained the O···H contact, which was labeled 1, and another red spot for the cocrystal was N···H contact, which was labeled 2. The shape index of the cocrystal is shown in Figure 10b; the curvedness is shown in Figure 10c. The intermolecular forces of O···H contact and N···H contact accounted for 17.1% and 6.3%, respectively. Analysis of the two-dimensional fingerprint plots showed that the most important interaction was H···H (40.5%) because of the large hydrogen-atom content of the cocrystal. In the pair of characteristic wings in the fingerprint plot, it was the interaction of C···H/H···C that contributed 27.6% to the Hirshfeld surface, which was contact of C−H···π. The interaction of C···C, which was π···π stacking, contributed 3.6% to the Hirshfeld surface. Therefore, the intermolecular forces that keep the cocrystal stable were mainly exerted by interaction of H···H and C···H/H···C.

https://doi.org/10.1021/acsomega.4c01136
ACS Omega 2024, 9, 31477−31487

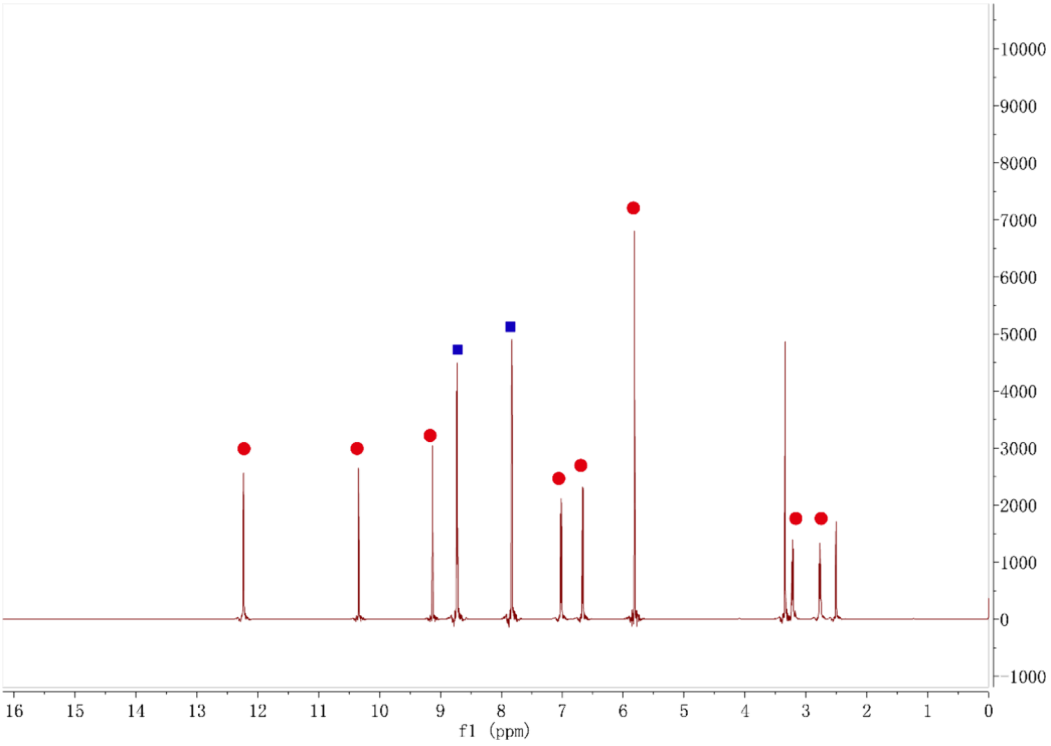

Figure 6. ^{1}HNMR of the Phl−4B cocrystal.

Table 1. Crystal Structure Parameters of the Phl−4B Cocrystal

compound	Phl−4B
chemical formula	$C_{25}H_{22}N_2O_5$
formula weight	430.44
temperature (K)	150(10)
λ (Å)	1.34138
crystal size (mm^3)	0.11 × 0.05 × 0.04
space group	P-1
crystal system	triclinic
a (Å)	7.6519(5)
b (Å)	9.7761(7)
c (Å)	14.4657(9)
α (°)	96.022(2)
β (°)	104.617(2)
γ (°)	90.117(2)
volume (Å^3)	1040.86(12)
Z	2
ρcalc (g·cm^{-3})	1.373
μ (mm^{-1})	0.509
2θ range	5.526−1130.142
F(000)	452
index ranges	$-10 \le h \le 10$
	$-13 \le k \le 13$
	$-19 \le l \le 19$
reflections collected	86,084
independent reflections	5264 [R_{int} = 0.0449, R_{sigma} = 0.0212]
data/restraints/parameters	5264/0/293
GOF	1.043
final R indexes [$I \ge 2\sigma$ (I)]	0.0410/0.1170
final R indexes (all data)	0.0431/0.1192
largest diff. peak/hole (e Å^{-3})	0.26/−0.23

Analysis of Solubility Experiments. For drugs with poor solubility, how to improve the solubility and dissolution behavior of drugs was an important research topic in the drug development stage. The solubility and dissolution rate of solid drugs were changed due to the formation of cocrystals, which affected the release and absorption of drugs in vivo. The solubility results of pure Phl were selected from the last experimental data.[16] According to the powder dissolution curve of the Phl−4B cocrystal (Figure 11), the cocrystal reached equilibrium solubility (49.93 ± 9.69 μg·mL^{-1}, P > 0.05) in pH 1.2 buffer for 540−1440 min. The equilibrium solubility in the cocrystal was significantly higher than that of the Phl raw material (4.38 ± 0.70 μg·mL^{-1}) and the mixture of Phl and 4B (22.34 ± 1.19 μg·mL^{-1}, both P < 0.05), respectively. The solubility of the Phl and 4B mixture was five times that of the Phl raw material. In pH 6.8 buffer, there was no statistical difference in solubility between the Phl−4B cocrystal and the Phl raw material during 540 to 1440 min (P > 0.05), indicating that the Phl and 4B cocrystal did not improve the solubility of Phl but the solubilities of both were higher than the solubility of the Phl and 4B mixture (P < 0.05). The "spring−parachute" effect of the Phl−4B cocrystal appeared in both buffers, and the Phl concentration in the Phl−4B cocrystal reached its peak value (68.46 ± 6.30 μg·mL^{-1}) at 15 min in pH 1.2 buffer and began to decrease. Furthermore, it began to decrease after the pH 6.8 buffer reached its peak value (32.41 ± 3.17 μg·mL^{-1}) at 75 min. This occurred because the hydrogen bonds within the cocrystal broke in solution, causing Phl to be released from the crystal structure and to transition into an amorphous state. Consequently, the concentration of Phl rose sharply at the beginning, exhibiting the "spring" effect. The amorphous form of Phl gradually precipitated from the solution, owing to its limited water solubility. Subsequently, the Phl concentration declined after reaching its peak, a phenomenon known as the

https://doi.org/10.1021/acsomega.4c01136
ACS Omega 2024, 9, 31477−31487

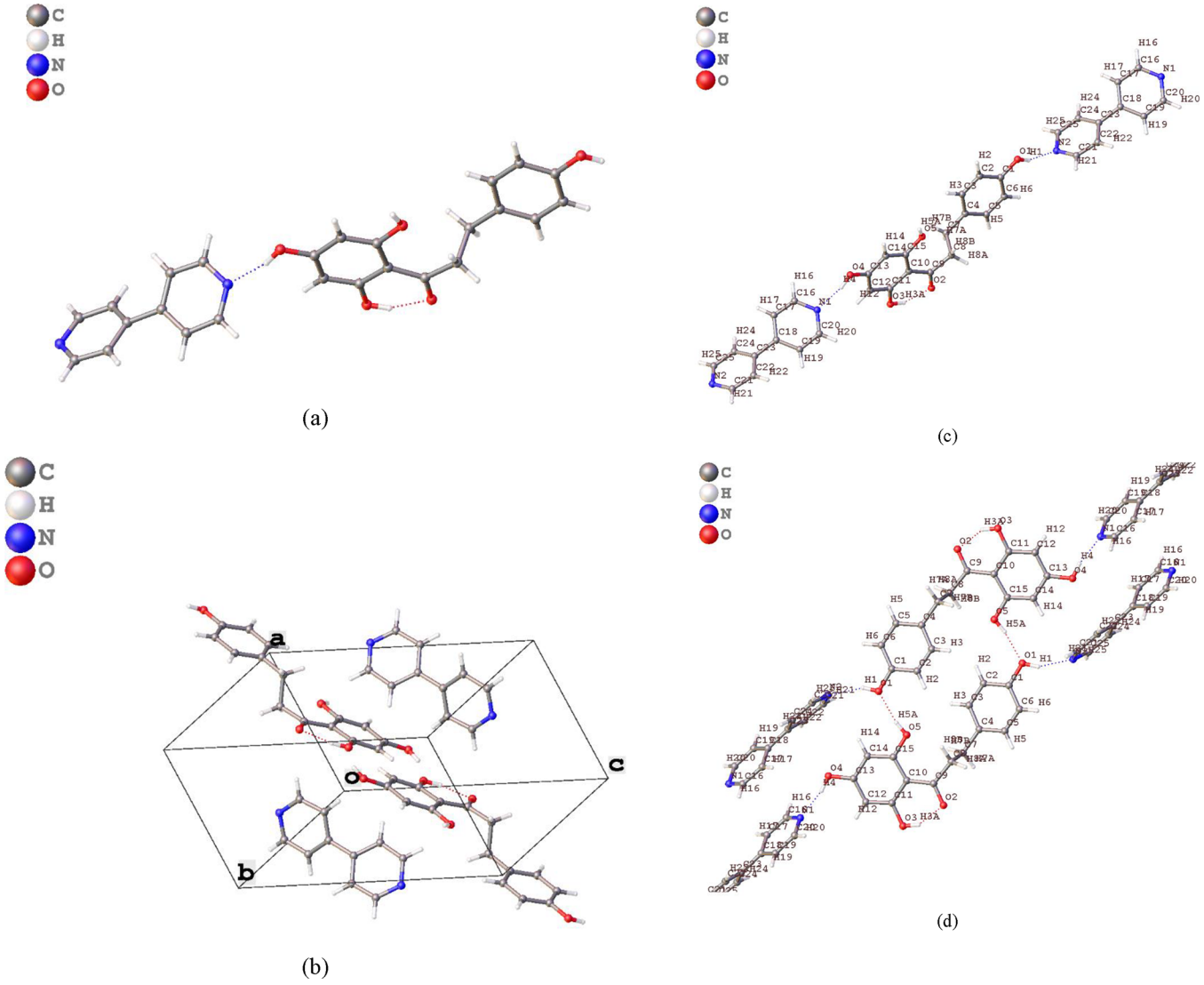

Figure 7. The Phl−4B cocrystal had an asymmetric unit (a), cell (b), one-dimensional plane (c), and two-dimensional plane (d).

Table 2. Hydrogen Bond Information of Phl−4B Cocrystal

hydrogen bond	H···A(Å)	D···A(Å)	D−H···A (°)
O1−H1...N2[a]	0.84	2.687(4)	156.0
O4−H4...N1	0.84	2.665(4)	165.9
O3−H3A···O2	0.84	2.489(3)	147.6
O5−H5A···O1[b]	0.84	2.742(4)	169.0

[a]Symmetry codes: 2+*X*,*Y*,−1+*Z*. [b]Symmetry codes: 2−*X*,−*Y*,−*Z*.

"parachute" effect. The alteration in the crystal structure significantly influenced the solubility of Phl. The results showed that the solubility of Phl in a pH 1.2 solution was improved after the formation of cocrystal Phl−4B.

***In Vitro* Digestive Simulation Experiment and Digestive Kinetics Analysis.** In vitro simulated digestion experiments of Phl and Phl−4B cocrystal were performed in simulated gastric fluid (SGF) and simulated intestinal fluid (SIF). The release rule of pure Phl was selected from the last experimental data.[16] According to Figure 12, the release rates of Phl and Phl−4B cocrystal at 120 min were 10.78% and 15.18%, respectively, during the incubation stage of gastric digestion, and the Phl−4B cocrystal release rate was significantly higher than that of the Phl raw material at this

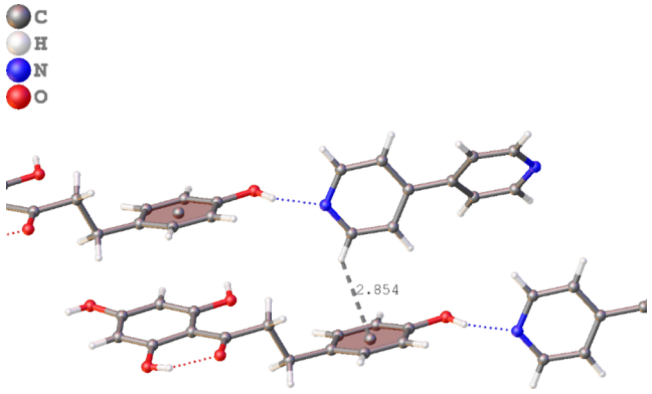

Figure 8. H···π stacking in the Phl−4B cocrystal.

stage ($P < 0.05$). However, the release rate of the Phl raw material was very low in the first 30 min and began to rise rapidly to 10.78% after 30 min. During the whole incubation period of small intestine digestion, the Phl raw material rapidly increased to 21.70% in the first 30 min and then slowly decreased to 17.59% in 360 min. The release rate of the Phl−4B cocrystal in 360 min was 19.5%. There was no significant

https://doi.org/10.1021/acsomega.4c01136
ACS Omega 2024, 9, 31477−31487

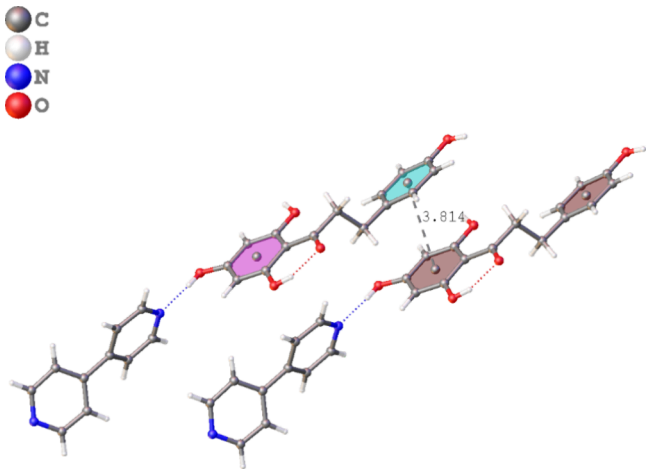

Figure 9. $\pi\cdots\pi$ stacking in the Phl−4B cocrystal.

difference in Phl release rate between the Phl−4B cocrystal and the Phl raw material ($P > 0.05$). The Phl−4B cocrystal had a higher Phl release rate in SGF compared to the Phl raw material but lower than that of the Phl raw material in SIF. In the solubility test, the Phl−4B cocrystal had a higher solubility than the Phl raw material at pH 1.2 but had no statistical difference with the Phl raw material at pH 6.8. The experimental results could correspond to the solubility experiment. In addition, the release rate of the Phl−4B cocrystal decreased at the later stage of the experiment, which may be due to the spring−parachute effect, in which the concentration of supersaturated Phl molecules was precipitated from the simulated digestive solution and the release rate decreased.

The fitting equation of the release kinetics model in Table 3 was fitted according to the release curves of the Phl raw material and the Phl−4B cocrystal.[31] The results showed that the Phl raw material and the Phl−4B cocrystal had the highest fit with the Ritger-Peppas model in these four kinetics models, and parameter n in the formula $Q = kt^n$ of this model was the drug release characteristic index: when $n \leq 0.45$, the drug release mechanism was mainly Fick diffusion. When $0.45 < n < 0.89$, the drug release was mainly caused by the combination of drug diffusion and skeleton dissolution. When $k \geq 0.89$, the drug release mechanism was skeleton dissolution. The fitting equations of Phl and Phl−4B cocrystal were $R = 1.4612t^{0.4561}$ and $R = 3.3255t^{0.2933}$, and their n values were 0.4561 and 0.2933, respectively, indicating that the release of Phl was mainly a synergistic effect of diffusion and outer wall dissolution. The release of Phl in the Phl−4B cocrystal was mainly due to Fick diffusion.[32] However, the correlation

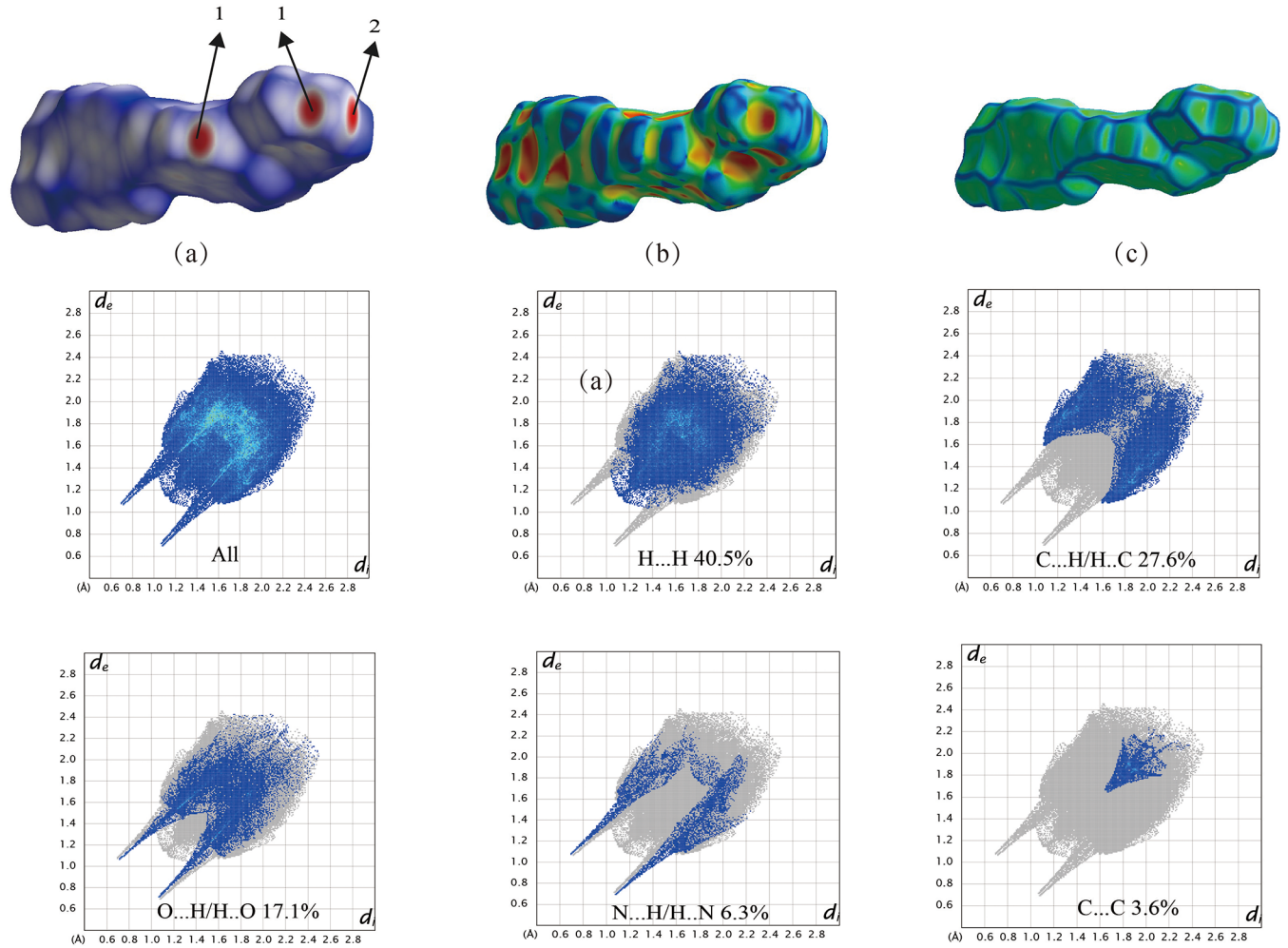

Figure 10. Picture of the Hirshfeld surfaces for the Phl−4B cocrystal (a). Hirshfeld mapped with shape index (b) and curvedness (c) and fingerprint plots for the cocrystal.

https://doi.org/10.1021/acsomega.4c01136
ACS Omega 2024, 9, 31477−31487

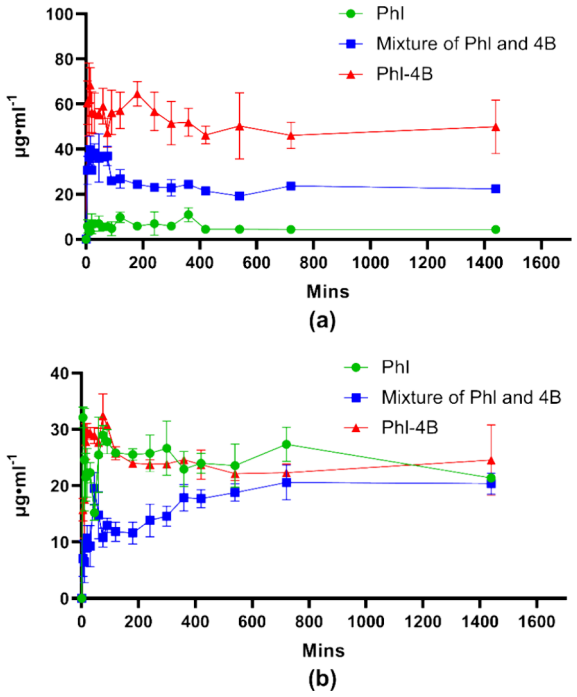

Figure 11. Solubility curves of Phl, 4B, and Phl−4B cocrystal in pH 1.2 (a) and 6.8 (b).

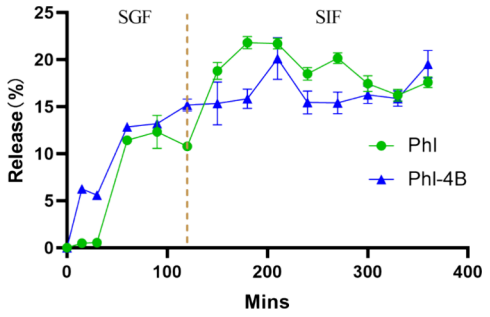

Figure 12. Release rule of Phl and Phl−4B cocrystal in the in vitro digestive simulation experiment.

Table 3. Phl and Phl−4B Cocrystal-Simulated Digestion Fitting Equations

compound	model	fitting equation	R^2
Phl	zero-order model	$R = 4.8466t + 0.05009$	0.5760
	first-order model	failed	
	Higuchi model	$R = 1.1878t^{1/2} - 0.5096$	0.7367
	Ritger-Peppas model	$R = 1.4612t^{0.4561}$	0.7390
Phl−4B	zero-order model	$R = 0.03696t + 7.1285$	0.6001
	first-order model	failed	
	Higuchi model	$R = 0.8801t^{1/2} - 3.0315$	0.8019
	Ritger-Peppas model	$R = 3.3255t^{0.2933}$	0.8662

coefficient of each model was not high and, it may not be the most optimal model for explaining the release curve. Additionally, other models were employed to fit the release curve in subsequent analyses. Phl's release behavior may be similar to that of the raw form because they both originate from the same type of crystal. However, the presence of 4B may affect the release behavior of Phl in a mixed model; we will investigate the release of Phl in mixed models in the future.

Stability Experiment. The physical and chemical stability of the compound in a cocrystal changes due to the changes in the arrangement and accumulation mode of the molecules. In this part, the phase and content changes of Phl and its cocrystal in 3 months were investigated. The results are shown in Figure 13a. The PXRD patterns of Phl raw materials and cocrystal did

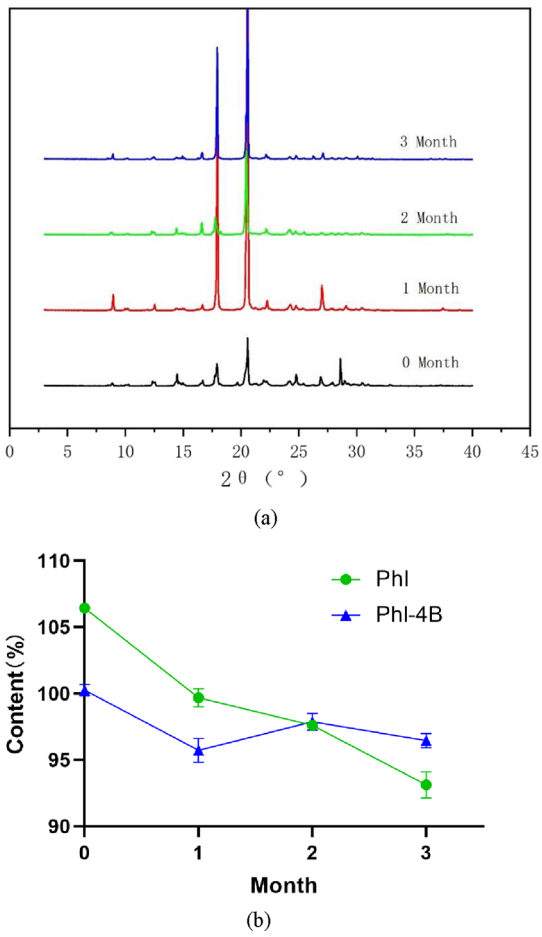

Figure 13. PXRD patterns of samples (a) for 3 months and the contents of samples changing in 3 months (b).

not change significantly within 3 months, indicating that the crystal phase did not change, and the crystal stability of the Phl−4B cocrystal and pPhl was good within 3 months at 40 °C, 75% RH.

While exploring the crystal stability, the concentration changes of Phl in the raw material and cocrystals were measured by HPLC (Figure 13b). Within 3 months, the content of the Phl raw material decreased from 106.443 ± 2.135% to 93.119 ± 7.965%. And the Phl content in the Phl−4B cocrystal decreased from 100.261 ± 3.514% to 96.452 ± 4.363%. The Phl content in the Phl−4B cocrystal was still significantly higher than that of the Phl raw material after the samples were placed at 40 °C, 75% RH, for 3 months ($P < 0.05$), indicating that the chemical stability of Phl after forming a cocrystal with 4B was better than that of the Phl raw material. The reason may be the change of crystal structure after the formation of the cocrystal and the change of intermolecular H···π stacking and hydrogen bond force, which makes the crystal structure more stable.

Antioxidant Activity. As shown in Figure 14, compared with the model group, the survival rate of H9C2 cells

https://doi.org/10.1021/acsomega.4c01136
ACS Omega 2024, 9, 31477−31487

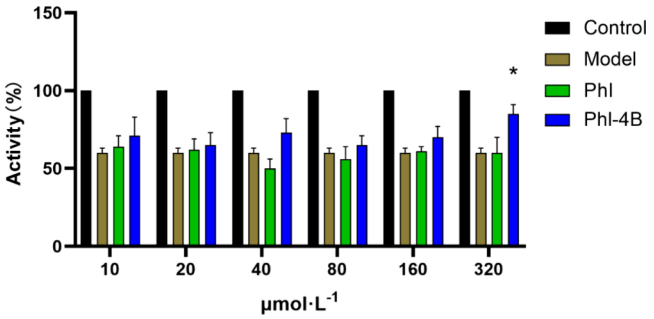

Figure 14. Antioxidant of Phl and the cocrystal in the test of H9C2 cells (*P < 0.05).

pretreated with Phl raw material showed no significant difference with that of the model group at different concentrations (P > 0.05). After treatment with Phl−4B, the survival rate of H9C2 cells at 320 μmol·L^{-1} was significantly improved compared with the model group (P < 0.05). This preliminarily proved that the antioxidant capacity of Phl was improved after forming a cocrystal with 4B. The better solubility of the cocrystal allows for more drug release so that the concentration of drugs is increased around the cell. Therefore, the antioxidant activity of the drug was improved after cocrystallization.

CONCLUSIONS

In this study, a solubilized cocrystal solution was innovatively employed to improve the water solubility of phloretin. The Phl−4B cocrystal was synthesized using the solvent evaporation method. Characterization of the Phl−4B cocrystal was conducted using PXRD, DSC, TGA, SCXRD, FTIR, ^{1}HNMR, and Hirshfeld surface analysis. The crystal structure, stoichiometric ratio, and intermolecular force of the two cocrystal materials were determined. Following the formation of the Phl−4B cocrystal, the solubility of Phl in a pH 1.2 environment improved, enhancing its stability. The release of Phl from the Phl−4B cocrystal was mainly due to Fick diffusion in an *in vitro* digestive simulation experiment. In the hypoxic reoxygenation model of H9C2 cells, it was observed that the antioxidant capacity of Phl was enhanced upon forming a cocrystal with 4B. The enhancement of antioxidant activity indicated that the formation of the cocrystal could alter the final pharmacological effect. Compared to the Phl−Inz cocrystal, the Phl−4B cocrystal had a new intermolecular force of $\pi\cdots\pi$ packing because the structure contained more six-membered rings. Therefore, we could consider using $\pi\cdots\pi$ stacking instead of hydrogen bonding when designing cocrystal synthesis strategies. Maintaining the structural integrity of Phl, addition of a suitable CCF could alter the spatial structure of Phl crystals, thereby enhancing the physicochemical properties and pharmacodynamic effects. This study provides both theoretical groundwork and practical insights for the future design and synthesis of novel solid formulations of Phl. Despite the toxicity of 4B, rendering it unsuitable for pharmaceutical applications,[33] the formation of the Phl−4B cocrystal suggests that Phl has the potential to form cocrystals with molecules containing pyridine groups, guiding future research in identifying suitable CCFs for cocrystal formation with Phl.

MATERIALS AND METHODS

Materials. Phl (purity ≥98%) and 4B (purity = 98%) were purchased from Shanghai Macklin Biochemical Co., Ltd. (Shanghai, China). Phloretin (HPLC ≥98%) was purchased from Shanghai Yuanye Biotechnology Co., Ltd. (Shanghai, China). Methanol was obtained from Guangzhou Reagent Co., Ltd. (Guangzhou, China). Simulated gastric fluid and simulated intestinal fluid were purchased from Guangzhou Testing Technology Co., LTD.(Guangzhou, China). The H9C2 cell was purchased from the Institute of Biochemistry and Cell Biology Sciences, Chinese Academy of Sciences (Shanghai, China). Penicillin−streptomycin, fetal bovine serum, phosphate-buffered saline, and DMEM high-glucose culture medium were from Gibco (Grand Island, New York). MTT (2-(4,5-dimethyl-2-thiazolyl)-3,5-diphenyl-2*H*-tetrazol-3-ium bromide) were purchased from Sigma-Aldrich (St Louis, Missouri).

Preparation of the Cocrystal. Phl and 4B were dissolved in 15 mL of methanol at a stoichiometric ratio of 1:1, followed by ultrasound until all solids were completely dissolved, and mixed in a parallel synthesizer (Carousel 6 Plus, UK) at a speed of 350 rpm for 12 h. After being mixed, the solution was transferred to the beaker and volatilized at room temperature for 3 to 5 days. When numbers of pink and needle crystals were precipitated from the liquid and attached to the wall and bottom of the beaker, the crystals were collected and transferred to a vacuum drying oven to dry at 45 °C for 8 h. Finally, the crystals were sealed in a refrigerator at 4 °C.

Powder X-ray Diffraction (PXRD). The powder X-ray diffraction test was performed on an X'Pert multifunctional powder X-ray diffractometer (PANalytical, Netherlands). The test was under the condition at 30 mA and 40 kV with Cu K_α radiation (λ = 1.540598 Å). The scanning range and wavelength were 3−40° and 0.131/step, respectively. Before the test, the powder of each sample was ground and crushed through a 100 mesh screen to ensure a uniform particle size.

Thermal Test. The thermal test of samples was tested by a DSC/DTA-TG STA 449 F5 Jupiter (NETZCH, Germany) instrument. The samples were tested in aluminum pans, respectively. The temperature rose from 30 to 500 °C with the rate of 10 °C/min. The protect gas and purge gas were N_2.

Fourier Transform Infrared Spectroscopy. The samples were dried at 45 °C for 6 h in a vacuum-drying oven before testing and then placed in a dryer overnight (desiccant is P_2O_5). The dried sample of 1−2 mg was weighed and scanned by a Fourier infrared spectrometer (PerkinElmer, United States). The scanning range was set to 4000−400 cm^{-1}, and the test ambient temperature was 25 °C.

^{1}HNMR. A 1 mg sample was weighed and thoroughly dissolved in 1 mL of DMSO-d_6 with TMS as an internal standard. Then, the samples were tested by a nuclear magnetic resonance spectrometer (Bruker, Germany) at 600 MHz at room temperature.

Single-Crystal X-ray Diffraction (SCXRD). The crystal structure of the Phl−4B cocrystal was determined by single-crystal X-ray diffraction. Data of the structure was collected by an Agilent SuperNova diffractometer with Ga Ka radiation (λ= 1.34138 Å) at 150 K. The data reduction and correction were performed by CrysAlis^{PRO}. The calculation of the crystal's structure was refined by Olex2 ShelXT[34] and ShelXL.[35] The pictures of the structure were drawn by Olex2.

https://doi.org/10.1021/acsomega.4c01136
ACS Omega 2024, 9, 31477−31487

Hirshfeld Surface Analysis of the Cocrystal. The molecular interaction of cocrystal asymmetric units was analyzed by CrystalExplorer 21.5.[36] The cocrystal Hirshfeld surface and corresponding fingerprints were generated from the structural data. The normalized contact distance (d_{norm}) surface of the fingerprint was mapped to a specified range of −0.6753−1.2005A.

HPLC Measurement. The Phl's concentration was examined by HPLC (Agilent 1200, USA) using an Agilent G1311A pump and an Agilent G1315D DAD. The chromatographic separation was performed on a Diamonsil C18 column (column 250 × 4.6 mm, 1.8 μm) at a flow rate of 1 mL·min^{-1} solution A (water) and solution C (acetonitrile), which were chosen as mobile phases. The gradient elution was set as follows: 40 - 60% C (0−12 min) and 60−40% C (12−15 min). The injection volume was 15 mL, and the detection wavelength was 273 nm.

Solubility Test. A shake-flask method was used to measure the solubility samples. The cocrystal and its mixture were tested in pH 1.2 ± 0.2 hydrochloric acid buffer and pH 6.8 ± 0.2 phosphate buffer solutions, respectively, which were placed in a penicillin bottle containing 10 mL of solution. The bottles were rotated at 37 ± 0.5 °C at 100 rpm for 24 h. 0.4 mL of liquid was extracted with a pipet, and 0.4 mL of buffer was replaced at 5, 10, 15, 20, 30, 45, 60, 75, 90, 120, 150, 180, 240, 300, 360, 420, 540, 720, and 1440 min. The concentration at each time point was detected by HPLC (n = 3).

In Vitro Digestive Simulation Experiment and Digestive Kinetics Study. Approximately 6 mg of samples was weighted, added with 4 mL of simulated gastric fluid, and stirred at 37 °C at 100 rpm·min^{-1}. After 2 h, the pH of the remaining digestive fluid was adjusted to 6.8 with NaOH and mixed with simulated intestinal fluid at a 1:1 (v/v) ratio. The release medium was stirred at 37 °C for 4 h and taken every 30 min. The concentration of Phl was detected by HPLC (n = 3). In order to further understand the release mechanism of phloretin in cocrystal digestive fluid in simulated gastroenteric fluid, the zero-order model, first-order model, Higuchi model, and Ritger−Peppas model were used to study the digestive kinetics,[37] which were calculated according to the following equations:

$$\text{zero} - \text{order model: } R = kt$$

$$\text{first} - \text{order model: } In(1 - R) = kt$$

$$\text{Higuchi model: } R = kt^{1/2}$$

$$\text{Ritger} - \text{Peppas model: } R = kt^{n}$$

R is the cumulative release rate of phloretin, k is the release coefficient, and n is the diffusion coefficient.

Stability Evaluation of Free Phl and the Cocrystal. In order to test the stability of Phl and the cocrystal, 30 mg of each sample (Phl, 4B, and cocrystal) was placed in the bottom of breakers and were stored for 90 days (40 °C, RH 75%). The purity of Phl was determined by HPLC, and the diffraction pattern was tested by PXRD.

Antioxidant Assay. H9C2 cells were cultured in DMEM high-glucose culture medium containing 10% fetal bovine serum and 1% double antibody at 37 °C and 5% CO_2. When H9C2 cells were cultured to the logarithmic growth stage, the cells were seeded and inoculated into 96-well plates with 2.0 × 10^4 cells per well for 24 h. The cells were divided into control group, model group, and drug group. Complete DMEM was used in the control group, and DMEM (without glucose) was used in the model group and drug group. The cells in the model group were placed in an anoxic box with 99% nitrogen content for 4 h. After 4 h, the culture medium was changed to DMEM and the cells were placed in an incubator at 37 °C and 5% CO_2 for 3h. The drug group was further divided into Phl group and cocrystal group, which were treated with various concentrations of Phl and cocrystal. After 7 days of continuous culture, 20 μL of MTT test solution (5 mg·mL^{-1}) was added to each well for 4 h, and 150 μL of DMSO solution was added to each well to shake well, and OD values were determined at 490 nm using a multifunctional enzyme labeler.

Statistical Analysis. Statistical analysis was performed with SPSS 25 and GraphPad 9.0.0 software. For measurement data, Shapiro−Wilk was used to test the normal distribution. If measurement data conform to normal distribution, mean ± standard deviation ($\bar{x} \pm s$) was used to describe the measurement data. The univariate ANOVA method was used for comparison between groups. The method of multiple comparison was Bonferroni correction.

■ ASSOCIATED CONTENT

Supporting Information

The Supporting Information is available free of charge at https://pubs.acs.org/doi/10.1021/acsomega.4c01136.

Crystallographic data (CCDC code 2326915) (CIF)

■ AUTHOR INFORMATION

Corresponding Authors

Yanfen Chen − *Guangdong Provincial Hospital of Chinese Medicine, Guangzhou 510120, China*; Phone: +86-20-81400801; Email: chenyanfen0479@126.com; Fax: +86-20-81400801

Wei Zhu − *The Second Affiliated Hospital, Guangzhou University of Chinese Medicine, Guangzhou 510120, China*; Phone: +86-20-39318571; Email: zhuwei9201@163.com; Fax: +86-20-39318571

Authors

Zhongyu Lu − *Guangdong Provincial Hospital of Chinese Medicine, Guangzhou 510120, China*; orcid.org/0000-0002-0177-0547

Gengzhen Yao − *Guangdong Provincial Hospital of Chinese Medicine, Guangzhou 510120, China*

Huanglie Xie − *Guangdong Provincial Hospital of Chinese Medicine, Guangzhou 510120, China*

Dawei Wang − *Shunde Hospital of Chinese Medicine of Foshan City, Foshan 528300, China*

Complete contact information is available at: https://pubs.acs.org/10.1021/acsomega.4c01136

Author Contributions

Z.L. was mainly responsible for experimental design, data analysis, picture drawing, and manuscript writing. All authors have made substantial contributions to the conception and design of the project. All authors have critically revised and approved the final submitted version of the manuscript.

Notes

The authors declare no competing financial interest.

https://doi.org/10.1021/acsomega.4c01136
ACS Omega 2024, 9, 31477−31487

■ ACKNOWLEDGMENTS

This research was funded by the Guangdong Provincial Hospital of Chinese Medicine Science and Technology Research Program (YN2023MS44), 2021 Foshan Key Project of Key Areas Science and Technology Research (2120001008478), the Project of State Key Laboratory of Dampness Syndrome of Traditional Chinese Medicine jointly built by the province in 2021 (SZ2021KF07), Guangzhou Science and Technology Projects (2023A03J0230) and Jiangxi Province Key Laboratory of Traditional Chinese Medicine-Pulmonary Science (2024SSY06321).

■ REFERENCES

(1) Abdelkader, H.; Fathalla, Z. Investigation into the Emerging Role of the Basic Amino Acid L-Lysine in Enhancing Solubility and Permeability of BCS Class II and BCS Class IV Drugs. *Pharm. Res.* **2018**, *35* (8), 160.

(2) Albetawi, S.; Abdalhafez, A.; Abu-Zaid, A. A Review on Recent Controlled Release Strategies for Oral Drug Delivery of Repaglinide (a BCS Class II Drug). *Pharmaceutical Nanotechnology* **2021**, *9* (5), 326−338.

(3) Pignatello, R.; Corsaro, R.; Bonaccorso, A.; Zingale, E.; Carbone, C.; Musumeci, T. Soluplus® polymeric nanomicelles improve solubility of BCS-class II drugs. *Drug Delivery and Translational Research* **2022**, *12* (8), 1991−2006.

(4) Blagden, N.; de Matas, M.; Gavan, P. T.; York, P. Crystal engineering of active pharmaceutical ingredients to improve solubility and dissolution rates. *Adv. Drug Delivery Rev.* **2007**, *59* (7), 617−630.

(5) Schultheiss, N.; Newman, A. Pharmaceutical cocrystals and Their Physicochemical Properties. *Cryst. Growth Des* **2009**, *9* (6), 2950−2967.

(6) Blagden, N.; Berry, D. J.; Parkin, A.; Javed, H.; Ibrahim, A.; Gavan, P. T.; De Matos, L. L.; Seaton, C. C. Current directions in co-crystal growth. *New J. Chem.* **2008**, *32* (10), 1659.

(7) Karagianni, A.; Malamatari, M.; Kachrimanis, K. Pharmaceutical cocrystals: New Solid Phase Modification Approaches for the Formulation of APIs. *Pharmaceutics* **2018**, *10* (1), 18.

(8) Guan, D.; Xuan, B.; Wang, C.; Long, R.; Jiang, Y.; Mao, L.; Kang, J.; Wang, Z.; Chow, S. F.; Zhou, Q. Improving the Physicochemical and Biopharmaceutical Properties of Active Pharmaceutical Ingredients Derived from Traditional Chinese Medicine through cocrystal Engineering. *Pharmaceutics* **2021**, *13* (12), 2160.

(9) Wang, N.; Xie, C.; Lu, H.; Guo, N.; Lou, Y.; Su, W.; Hao, H. cocrystal and its Application in the Field of Active Pharmaceutical Ingredients and Food Ingredients. *Curr. Pharm. Des.* **2018**, *24* (21), 2339−2348.

(10) Hsiao, Y.-H.; Hsieh, M.-J.; Yang, S.-F.; Chen, S.-P.; Tsai, W.-C.; Chen, P.-N. phloretin suppresses metastasis by targeting protease and inhibits cancer stemness and angiogenesis in human cervical cancer cells. *Phytomedicine* **2019**, *62*, No. 152964.

(11) Hytti, M.; Ruuth, J.; Kanerva, I.; Bhattarai, N.; Pedersen, M. L.; Nielsen, C. U.; Kauppinen, A. phloretin inhibits glucose transport and reduces inflammation in human retinal pigment epithelial cells. *Mol. Cell. Biochem.* **2023**, *478* (1), 215−227.

(12) Alsanea, S.; Gao, M.; Liu, D. phloretin Prevents High-Fat Diet-Induced Obesity and Improves Metabolic Homeostasis. *AAPS Journal* **2017**, *19* (3), 797−805.

(13) Li, B.; Xu, L.; Liu, J.; Zhou, M.; Jiang, X. phloretin ameliorates heart function after myocardial infarction via NLRP3/Caspase-1/IL-1β signaling. *Biomed. Pharmacother.* **2023**, *165*, No. 115083.

(14) Deshpande, R. D.; Shah, D. S.; Gurram, S.; Jha, D. K.; Batabyal, P.; Amin, P. D.; Sathaye, S. Formulation, characterization, pharmacokinetics and antioxidant activity of phloretin oral granules. *Int. J. Pharm.* **2023**, *645*, No. 123386.

(15) Mao, W.; Fan, Y.; Wang, X.; Feng, G.; You, Y.; Li, H.; Chen, Y.; Yang, J.; Weng, H.; Shen, X. phloretin ameliorates diabetes-induced endothelial injury through AMPK-dependent anti-EndMT pathway. *Pharmacol. Res.* **2022**, *179*, No. 106205.

(16) Lu, Z.; Chen, H.; Mo, J.; Yuan, X.; Wang, D.; Zheng, X.; Zhu, W. cocrystal of phloretin with isoniazid: preparation, characterization, and evaluation. *RSC Adv.* **2023**, *13* (16), 10914−10922.

(17) He, Y.; Chen, S.; Li, M.; Gao, Y.; Feng, H.; Umar, Q.; Yin, D.; Feng, Y. Novel co-crystal of 3-methylcinnamic acid with berberine (1:1): synthesis, characterization, and intestinal absorption property. *Drug Dev. Ind. Pharm.* **2023**, *49* (10), 617−627.

(18) Vasoya, J. M.; Lee, H. L.; Lee, T.; Serajuddin, A. T. M. Continuous Synthesis of Cinnarizine Salt with Malic Acid by Applying Green Chemistry Using Water-Assisted Twin Screw Extrusion. *Mol. Pharmaceutics* **2023**, *20* (10), 5160−5172.

(19) Yang, C.; Guo, W.; Lin, Y.; Lin, Q.; Wang, J.; Wang, J.; Zeng, Y. Experimental and DFT simulation study of a novel felodipine cocrystal: Characterization, dissolving properties and thermal decomposition kinetics. *J. Pharm. Biomed. Anal.* **2018**, *154*, 198−206.

(20) Chadha, R.; Bhalla, Y.; Nandan, A.; Chadha, K.; Karan, M. Chrysin cocrystals: Characterization and evaluation. *J. Pharm. Biomed. Anal.* **2017**, *134*, 361−371.

(21) Sawatdee, S.; Atipairin, A.; Rakkummerd, S.; Suriyaphol, O.; Harding, D. J.; Muenraya, P.; Harding, P. Preparation and physicochemical characterization of sildenafil cocrystals. *J. Adv. Pharm. Technol. Res.* **2021**, *12* (4), 408.

(22) Liu, M.; Hong, C.; Yao, Y.; Shen, H.; Ji, G.; Li, G.; Xie, Y. Development of a pharmaceutical cocrystal with solution crystallization technology: Preparation, characterization, and evaluation of myricetin-proline cocrystals. *Eur. J. Pharm. Biopharm.* **2016**, *107*, 151−159.

(23) Zhang, Y.; Du, X.; Wang, H.; He, Z.; Liu, H. Sacubitril-valsartan cocrystal revisited: role of polymer excipients in the formulation. *Expert Opinion on Drug Delivery* **2021**, *18* (4), 515−526.

(24) Qiao, N.; Li, M.; Schlindwein, W.; Malek, N.; Davies, A.; Trappitt, G. Pharmaceutical cocrystals: an overview. *Int. J. Pharm.* **2011**, *419* (1−2), 1−11.

(25) Sokal, A.; Pindelska, E.; Szeleszczuk, L.; Kolodziejski, W. Pharmaceutical properties of two ethenzamide-gentisic acid cocrystal polymorphs: Drug release profiles, spectroscopic studies and theoretical calculations. *Int. J. Pharm.* **2017**, *522* (1−2), 80−89.

(26) Metherall, J. P.; Carroll, R. C.; Coles, S. J.; Hall, M. J.; Probert, M. R. Advanced crystallisation methods for small organic molecules. *Chem. Soc. Rev.* **2023**, *52* (6), 1995−2010.

(27) Yang, T.; Willhammar, T.; Xu, H.; Zou, X.; Huang, Z. Single-crystal structure determination of nanosized metal−organic frameworks by three-dimensional electron diffraction. *Nat. Protoc.* **2022**, *17* (10), 2389−2413.

(28) Nirmal Ram, J. S.; Sathya, U.; Gomathi, S.; Cordes, D. B. Structure determination and Hirshfeld surface analysis of new cocrystal and salt forms of 5-aminotetrazole with hydroxy- and nitro-substituted carboxylic acids. *Acta Crystallographica Section C Structural Chemistry* **2022**, *78* (7), 414−423.

(29) Habuka, Y.; Takeuchi, E. A.; Hori, A. Co-crystal structure, Hirshfeld surface analysis and DFT studies of 3,4-ethylenedioxythiophene solvated bis[1,3-bis(pentafluorophenyl)propane-1,3-dionato]-copper(II). *Acta Crystallographica Section E Crystallographic Communications* **2020**, *76* (6), 820−825.

(30) Parwani, A. V. Expression of Glypican 3 in Ovarian and Extragonadal Germ Cell Tumors. *Yearbook of Pathology and Laboratory Medicine* **2009**, *2009*, 93−95.

(31) Tiew, S. X.; Misran, M. Encapsulation of salicylic acid in acylated low molecular weight chitosan for sustained release topical application. *J. Appl. Polym. Sci.* **2017**, *134* (36), 44849.

(32) Liu, Y.; Zhang, J.; Sheng, X.; Li, N.; Ping, Q. Adsorption and Release Kinetics, Equilibrium, and Thermodynamic Studies of Hymexazol onto Diatomite. *ACS Omega* **2020**, *5* (45), 29504−29512.

(33) Bruni, G.; Maggi, L.; Monteforte, F.; Ferrara, C.; Capsoni, D.; Berbenni, V.; Milanese, C.; Girella, A.; Friuli, V.; Mustarelli, P.; Marini, A. Zaltoprofen/4,4′-Bipyridine: A Case Study to Demonstrate

https://doi.org/10.1021/acsomega.4c01136
ACS Omega 2024, 9, 31477−31487

the Potential of Differential Scanning Calorimetry (DSC) in the Pharmaceutical Field. *J. Pharm. Sci.* **2021**, *110* (11), 3690−3701.
(34) Sheldrick, G. M. SHELXT− Integrated space-group and crystal-structure determination. *Acta Crystallographica Section A Foundations and Advances* **2015**, *71* (1), 3−8.
(35) Sheldrick, G. M. Crystal structure refinement withSHELXL. *Acta Crystallographica Section C Structural Chemistry* **2015**, *71* (1), 3−8.
(36) Spackman, P. R.; Turner, M. J.; McKinnon, J. J.; Wolff, S. K.; Grimwood, D. J.; Jayatilaka, D.; Spackman, M. A. CrystalExplorer: a program for Hirshfeld surface analysis, visualization and quantitative analysis of molecular crystals. *J. Appl. Crystallogr.* **2021**, *54* (3), 1006−1011.
(37) Wang, P.-P.; Luo, Z.-G.; Peng, X.-C. Encapsulation of Vitamin E and Soy Isoflavone Using Spiral Dextrin: Comparative Structural Characterization, Release Kinetics, and Antioxidant Capacity during Simulated Gastrointestinal Tract. *J. Agric. Food Chem.* **2018**, *66* (40), 10598−10607.

https://doi.org/10.1021/acsomega.4c01136
ACS Omega 2024, 9, 31477−31487